

RESEARCH ARTICLES

OPTICS

Shrinking light to allow forbidden transitions on the atomic scale

Nicholas Rivera,^{1*} Ido Kaminer,^{1*} Bo Zhen,² John D. Joannopoulos,¹ Marin Soljačić¹

The diversity of light-matter interactions accessible to a system is limited by the small size of an atom relative to the wavelength of the light it emits, as well as by the small value of the fine-structure constant. We developed a general theory of light-matter interactions with two-dimensional systems supporting plasmons. These plasmons effectively make the fine-structure constant larger and bridge the size gap between atom and light. This theory reveals that conventionally forbidden light-matter interactions—such as extremely high-order multipolar transitions, two-plasmon spontaneous emission, and singlet-triplet phosphorescence processes—can occur on very short time scales comparable to those of conventionally fast transitions. Our findings may lead to new platforms for spectroscopy, sensing, and broadband light generation, a potential testing ground for quantum electrodynamics (QED) in the ultrastrong coupling regime, and the ability to take advantage of the full electronic spectrum of an emitter.

A fundamental process in the field of light-matter interaction is spontaneous emission, in which an excited electron in an atom lowers its energy by emitting light (1–3). Spontaneous emission is responsible for the characteristic emission spectrum of an emitter. In principle, an excited electron can fall into any unoccupied lower energy level via this process. In practice, the majority of radiative decay channels are too slow to be accessible, rendering most of the spectrum invisible and inaccessible. The wealth of forbidden light-matter interaction processes can be appreciated by considering three very general classes of forbidden transitions: multipolar processes, spin-flip processes, and multi-quanta emission processes.

Multipolar transitions are those in which the orbital angular momentum (OAM) quantum number of the electron changes by more than one unit. The transitions are slow because the wavelength of emitted light (around 10^3 to 10^5 Å) is typically far larger than the size of the atomic or molecular orbitals participating in the transition (around 1 to 10 Å). As a result of this difference in length scales, the rates of electronic transitions as a function of angular momentum vary over many orders of magnitude: The difference in rates between changing OAM by 1 and changing OAM by 5 can be more than 20 orders of magnitude, making high OAM transitions invisible in the absorption and emission spectrum of an emitter. The ability to access these transitions would allow a multiplexed and broadband spectroscopy platform, in which

much more of the electronic energy level structure of an emitter can be probed using light.

A spin-flip process is one in which the spin of the electron flips as a result of the emission. Common spin-flip processes include those in which a single electron flips its spin and those in which a pair interconverts between a singlet and triplet state. Because these processes are very slow, spin-flip processes typically occur through phosphorescence, which is fast only when the electrons experience large spin-orbit coupling (4, 5). In systems where spin-orbit coupling is weak, such as in atoms or hydrocarbon molecules, the radiative quantum yield of phosphorescence is low because the singlet-triplet transition is much slower than nonradiative recombination processes. This is undesirable for applications such as organic-based light-emitting diodes where high radiative quantum efficiency is desired.

Multiquanta emission processes are those in which an electron lowers its energy by emitting two or more quanta of light. This is a higher-order process in QED. Although it is not forbidden by dipole selection rules, it is typically so slow that we group it with the other two processes above. Because of the small size of the atom relative to the light it emits, and the small value of the fine-structure constant, emission of even two quanta tends to be slower than the emission of a single quantum of light by 8 to 10 orders of magnitude. This makes two-quanta spontaneous emission processes notoriously difficult to observe. Two-photon spontaneous emission was predicted in the early 1930s (6) but was not directly observed until 1996, in hydrogen (7). Going beyond atomic physics, two-quanta spontaneous emission processes are also of interest in semiconductors, where they were first observed in 2008 (8, 9). Enabling two-quanta spontaneous emission pro-

cesses at a fast rate would enable generation of entangled light, which is of great interest for implementing quantum protocols (10). It would also enable new broadband absorbers and novel broadband light sources using atomic and molecular emitters.

Despite the motivation to access all of these transitions, it is in practice very difficult. Conservation of energy and angular momentum dictates that in order to access the full spectrum of an emitter, it must couple to light, which, over a broad range of frequencies in the infrared-visible range, has wavelengths on the order of 1 to 5 nm (once inside an optical material). The wavelength of light and its frequency are related by the phase velocity. Thus, to access forbidden transitions, phase velocities of light on the order of $0.001c$ are required. Recent theoretical and experimental work has shown that systems such as graphene, silver monolayers, and beryllium surfaces can support precisely such strongly confined light in the form of plasmons. These two-dimensional (2D) systems have the unique ability to squeeze the wavelength of light by more than two orders of magnitude, which allows us to recast the main assumptions for light-matter interactions.

We report that through the use of 2D plasmons (11–24), which shrink the wavelength of light by more than two orders of magnitude, we can overcome all of the mentioned conventional limitations of light-matter interactions. In particular, we show by means of a general theory of atom-plasmon interactions that the rates of high-order multipolar transitions, two-plasmon spontaneous emission, and spin-flip transition rates become enhanced to the point that they are comparable to dipole transition rates and thus become straightforwardly accessible. For achievable plasmon confinements in graphene and other 2D plasmon-supporting materials, all of the previously forbidden transitions listed above can now have lifetimes within the range of 1 μs to 1 ns; these previously forbidden transitions can be made to be quite efficient, even when competing with conventionally allowed transitions. We analyze the effect of non-radiative quenching extensively and find that in many cases of interest, the radiation into plasmons is dominant and thus could be harvested as far-field light through suitable outcoupling techniques.

2D plasmons and light-matter interaction: Model and assumptions

Plasmons are understood in the framework of classical electrodynamics as the coherent propagation of surface charge associated with tightly confined electromagnetic fields. The dispersion relation of any plasmon can be most simply expressed as

$$\omega = v_p q \equiv \frac{cq}{\eta(q)} \quad (1)$$

where q is the plasmon wave vector, v_p is the phase velocity, and η is the confinement factor, which is equal to both c/v_p and $\lambda_0/\lambda_{\text{pl}}$. The fact peculiar to 2D plasmons is that their wavelength λ_{pl} , which is determined by the dispersion relation, can be shorter than the wavelength of a free-space

¹Department of Physics, Massachusetts Institute of Technology, Cambridge, MA 02139, USA. ²Research Laboratory of Electronics, Massachusetts Institute of Technology, Cambridge, MA 02139, USA.

*These authors contributed equally to this work.

†Corresponding author. Email: nriviera@mit.edu

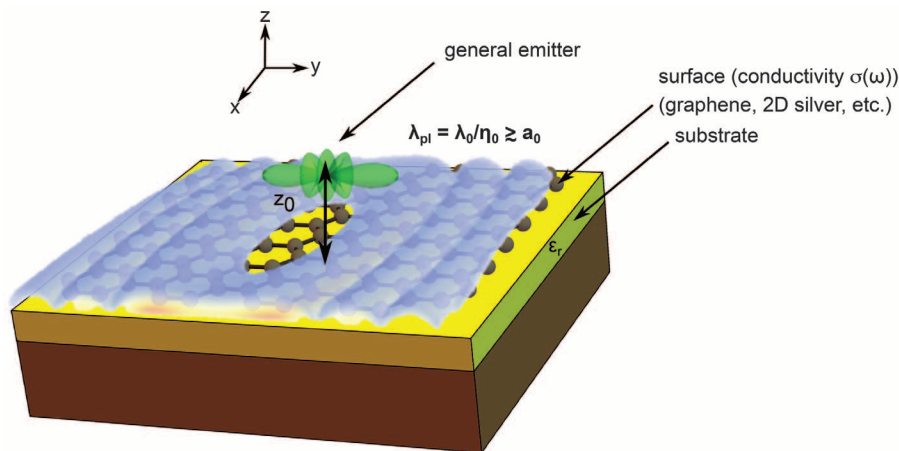


Fig. 1. Two-dimensional plasmons coupled to an emitter. A schematic of an emitter (not necessarily dipolar) above a 2D material of conductivity $\sigma(\omega)$ supporting plasmons with wavelength λ_{pl} , which is far shorter than the photon wavelength λ_0 (by a factor of η_0) and approaches the atomic size a_0 .

photon λ_0 at the same frequency by a factor of 100 to 400.

One 2D plasmonic platform of recent interest is graphene, in which the confinement factor has been predicted to be as high as 300 (15); values in excess of 200 have been indirectly observed below the intraband regime (23), values of 150 have been directly observed with low losses (21), and values of 240 have been observed in the interband regime (13). Yet other 2D plasmonic platforms exist; what is less well known is that even more highly confined plasmons can exist in other 2D electron systems such as metallic monolayers. In other 2D plasmons such as monolayer silver, confinement factors as high as 300 have been observed, corresponding to plasmon wavelengths of ~ 5 nm at photon wavelengths of $1.5 \mu\text{m}$ (11). On the surface of beryllium, acoustic plasmons have been observed at visible frequencies (~ 560 nm) with plasmon wavelengths of merely 1.5 nm (12), corresponding to confinement factors near 370. In our study, we look at the emission of 2D plasmons by hydrogen-like and helium-like atomic emitters in the vicinity of a 2D plasmonic system given by the minimally coupled Hamiltonian

$$\begin{aligned}
 H &= H_a + H_{em} + H_{int} \\
 H_a &= \left(\sum_i \frac{\mathbf{p}_i^2}{2m_e} - \frac{e^2}{4\pi\epsilon_0 r_i} \right) + H_{e-e} + H_{SO} \\
 H_{em} &= \sum_{j=x,y,z} \int d\mathbf{r} \int d\omega \hbar\omega \left[f_j^\dagger(\mathbf{r}, \omega) f_j(\mathbf{r}, \omega) + \frac{1}{2} \right] \\
 H_{int} &= \sum_i \frac{e}{2m_e} [\mathbf{p}_i \cdot \mathbf{A}(\mathbf{r}_i) + \mathbf{A}(\mathbf{r}_i) \cdot \mathbf{p}_i] + \\
 &\quad \frac{e^2}{2m_e} \mathbf{A}^2(\mathbf{r}_i) + \frac{e\hbar}{2m_e} \sigma_i \cdot \mathbf{B}(\mathbf{r}_i) \quad (2)
 \end{aligned}$$

where e is the electronic charge, m_e is the electron mass, \hbar is the Planck constant divided by 2π , \mathbf{A} and \mathbf{B} are the vector potential and magnetic field, \mathbf{r}_i denotes the position of the i th electron, σ_i denotes the spin of the i th electron,

H_{SO} is the spin-orbit coupling, and H_{e-e} is the electron-electron interaction. The $f_j^\dagger(\mathbf{r}, \omega)$ and $f_j(\mathbf{r}, \omega)$ are operators that respectively create and annihilate elementary excitations of the electromagnetic field in dissipative media. These excitations can be thought of as oscillating dipoles at position \mathbf{r} and frequency ω , oriented along direction j . The features of the plasmon and emitter relevant to our calculations are shown schematically in Fig. 1. This Hamiltonian, with field operators that appropriately describe the (potentially very high) losses in these confined plasmons, is sufficient to capture the fundamentally quantum nature of plasmons, which has been confirmed by experiments (25). This Hamiltonian describes both radiative decay and nonradiative decay mediated by interactions between the electromagnetic field and the orbital and spin degrees of freedom of the electron in an atom. It therefore describes intercombination transitions, multiplasmon emission, and other higher-order processes in the perturbation theory. In particular, this formalism makes predictions that (among others) give the correct Purcell factors for one-photon spontaneous emission of dipole emitters (26, 27), describe experimentally observed loss-induced quenching phenomena (20, 28), and describe experimentally observed two-plasmon phenomena as in (9).

We examined all of these interaction processes in order to provide a broad picture of atom-light interactions in plasmonics (29). We selected hydrogen- and helium-like emitters for definiteness, but the basic physics behind our results can readily be extended to any other atomic and molecular system. Although we explicitly consider only spontaneous emission, our results hold equally well for the absorption of excited 2D plasmons. Our approach can be applied to plasmons in 2D conductors with any general dispersion relation (for which the Drude model is a representative example that we consider). Our model can be generalized to consider nonlocal effects (30) by modifying the Green function formalism, which is done by replacing the local

conductivity $\sigma(\omega)$ by the nonlocal conductivity $\sigma(\mathbf{q}, \omega)$ everywhere. For the most part, our claims can be chosen to apply within the local-response regime of graphene, for easily achievable values of the Fermi energy E_F of graphene. We explicitly consider the nonlocal response of graphene [via the zero-temperature random phase approximation (RPA) (15, 27)] when we discuss two-plasmon spontaneous emission.

Multipolar transitions

The first class of forbidden transitions that we analyze consists of multipolar transitions in which the OAM of the electron changes by more than 1. It is well known that in conventional photonics and even plasmonics, electric dipole transitions are the fastest type of transitions and are thus appropriately the main object of study in the field of light-matter interactions. Electric quadrupole and magnetic dipole transitions, which are the second fastest types of transitions, are fairly slow but can be observed through conventional spectroscopic approaches (31) or in mesoscopic emitters such as quantum dots. Substantial theoretical and experimental efforts have gone toward speeding up these two processes (32–39). On the other hand, electric octupole, magnetic quadrupole, and higher-order multipolar transitions are far too slow to observe for small emitters such as atoms and molecules. Because of this, appreciable theoretical and experimental efforts have not been directed at speeding up such processes. Nevertheless, the spectrum of an atom associated with high-lying energy levels consists of precisely these types of transitions. Because of the high confinements achievable in 2D plasmons, transitions whose lifetimes in free space approach the age of the universe can be brought down to lifetimes of hundreds of nanoseconds, corresponding to a rate enhancement (defined as the Purcell factor) of nearly 10^{24} , as we demonstrate below. Such lifetimes are of the same order of magnitude as dipole transitions in free space and therefore should be straightforwardly accessible through absorption spectroscopy.

We calculate the rates of transitions where the electron OAM changes by n (an En transition) (29). The decay rate Γ_n into plasmons scales with η_0 as

$$\Gamma_n \sim \eta_0^{3+2(n-1)} \exp(-2\eta_0 k z_0) \quad (3)$$

where $k = 2\pi/\lambda_0$, and η_0 is the confinement factor at the transition frequency. Equation 3 makes it very clear that higher electric multipole transitions are enhanced by successively larger amounts. For achievable confinement factors of 100, when n increases by 1, the enhancement increases by a factor of roughly 10,000. Therefore, one should expect that if the dipole transitions ($n = 1$) are enhanced by 10^6 , then E2, E3, E4, and E5 transitions should be enhanced by factors of 10^{10} , 10^{14} , 10^{18} , and 10^{22} , respectively. One feature of Eq. 3 is that for high-order multipolar transitions, the decay rates have an extremely sharp dependence on the confinement. For example, with E5 transitions, where the rates of surface plasmon launching scale as η_0^{11} , a

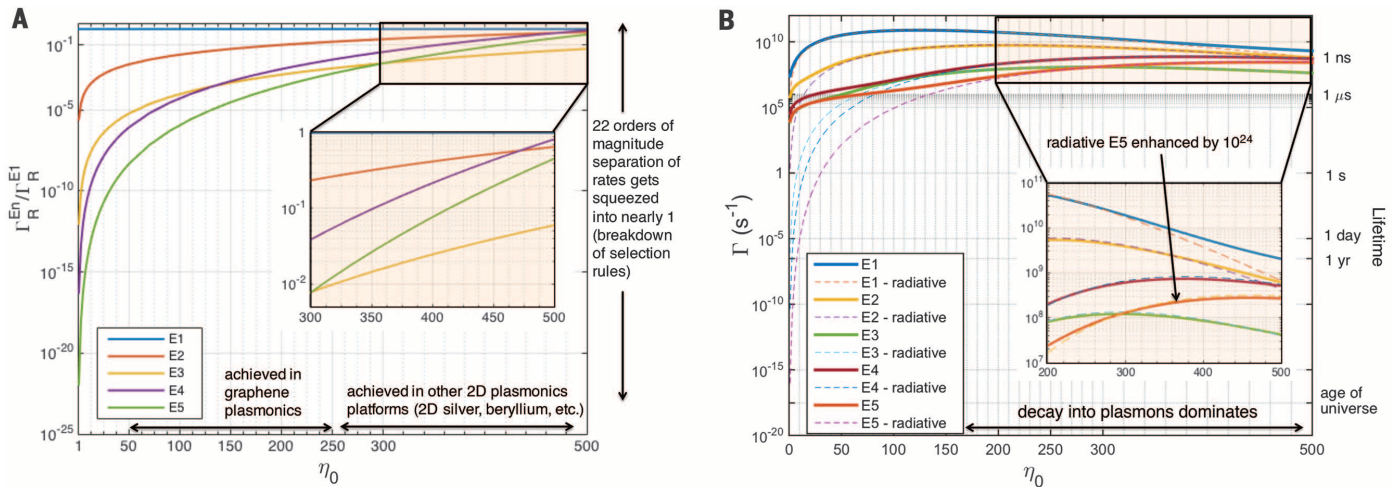


Fig. 2. Convergence of the multipoles. (A) Rates of radiation into surface plasmons for various multipolar transitions in hydrogen. The transition series considered here is $6\{p, d, f, g, h\} \rightarrow 4s$, which are E1 to E5 transitions, respectively. The free-space wavelengths of the transitions are all $2.6 \mu\text{m}$. The emitter is situated 5 nm above the surface of graphene. (B) Total rates (radiative + nonradiative) of decay for the same transition series in hydrogen (for a fixed quality factor of 5). Dashed lines show radiative rates, which agree with the total rates at high confinement.

change in the confinement factor by a factor of 2 can change the decay rates by more than three orders of magnitude.

The expression above can be intuitively reasoned as follows: The factor $\eta_0^3 \exp(-2\eta_0 k z_0)$ is proportional to the local photonic density of states (LDOS), reflecting the well-known fact that plasmon confinement can lead to very fast dipole transitions (26, 27, 40). The additional factors of η_0 that depend on the multipolar order of the transition are field-gradient enhancement factors. In particular, if we expand the plasmonic plane wave as

$$\exp(i\mathbf{q} \cdot \boldsymbol{\rho} - qz) = 1 + (i\mathbf{q} \cdot \boldsymbol{\rho} - qz) + \frac{1}{2!} (i\mathbf{q} \cdot \boldsymbol{\rho} - qz)^2 + \dots \quad (4)$$

we see that each term, which corresponds to some number of gradients of the electromagnetic field, can be mapped to particular multipolar transitions for wavelengths not too close to the atomic radius. Because $q = \eta_0(\omega/c)$, it is clear that each multipolar order is enhanced (relative to the dipole order) by some even power of η_0 and that this η_0 is proportional to the gradient of the electromagnetic field.

Such an intuition is confirmed in Fig. 2, where we plot the exact transition rates, with and without plasmonic losses, for the series of transitions $6\{p, d, f, g, h\} \rightarrow 4s$ in the hydrogen atom. The free-space wavelength of the transition is $2.6 \mu\text{m}$. In our simulations, the emitter is kept 5 nm away from the surface. We do not include the $6s \rightarrow 4s$ rate because, for the parameters under consideration, it is extremely small when the atom is well separated from the surface because of the approximate transversality of the electromagnetic field ($\nabla \cdot \mathbf{E} = 0$) (41). The dominant decay mechanism for this process will be two-plasmon emission, which we compute below. In Fig. 2A, we plot the radiative rates (i.e., plasmon emission rates, denoted Γ_R) of transitions in the hydrogen $6 \rightarrow 4$ series relative to the radiative rate

of the dipole transition (at the same energy) as a function of confinement. This relative rate is independent of atom-surface separation, as can be seen from Eq. 3. To give a particular example, conventionally the E5 transition is separated from the E1 transition by ~ 22 orders of magnitude. The free-space rate of the E5 transition is around 10^{-16} s^{-1} , corresponding to a lifetime that is two orders of magnitude less than the age of the universe. In contrast, for high confinement ($\eta_0 \approx 200$), the rate is $\sim 10^7 \text{ s}^{-1}$, which is more than an order of magnitude faster than the free-space E1 transition. Moreover, at this confinement, the entire multipolar series is separated by only three orders of magnitude (in rates), as opposed to 22 orders of magnitude in free space. A confinement of 200 is easily achievable in graphene in its local-response regime. For example, by tuning E_F to 0.4 eV , this 0.47-eV transition has a confinement of 200 when placed above a substrate with a relative permittivity of 4. Thus, it is possible to allow highly forbidden transitions in the local regime of graphene.

In addition to plotting confinement factors up to 200, we also plot confinement factors that are higher than have been observed in graphene below the interband regime. This is because such high confinement factors have been observed in plasmons in monolayer silver, DySi_2 , graphene with high losses, and acoustic plasmons in beryllium (11–14). We plot up to very high confinement factors of 500, corresponding to plasmon wavelengths of 5 nm . At these low wavelengths, which have been observed in the aforementioned systems, four of the five transitions in the series lie within the same order of magnitude, corresponding to a complete breakdown of the conventional selection rules. Another reason to plot for high confinement factors (even for graphene) is that it has recently been suggested via a modified RPA scheme that confinements above 300 may be possible with relatively low losses (42). Technically, in these highly confined plasmons with

linear dispersion, the quality factors Q have been observed to be quite low (of order unity). Figure 2B assumes a fixed Q of 5 throughout different confinement factors. If $Q = 1$, rates are, of course, quantitatively modified but remain within the same order of magnitude as in Fig. 2B, preserving our conclusion that these highly confined plasmons can break the selection rules completely. Moreover, it tells us that even despite very high losses of these plasmons, they can still completely reshape the dynamics of excited electrons in emitters. Therefore, these highly lossy plasmons have clear experimental consequences, even if they cannot be coupled out into free space. We discuss these consequences below.

In addition to radiation into plasmons, an excited emitter can be nonradiatively quenched by a conductor. Nonradiative quenching channels can include, but are not limited to, phonons, particle-hole excitations, and impurities. These are incorporated in our macroscopic QED calculations through the real part of the surface conductivity. Strictly speaking, because macroscopic QED sees only the total conductivity, it considers only the total quenching (by which we mean total nonradiative decay). Therefore, we cannot isolate the quenching sources, but we may still compare the total quenching to the total plasmon emission. In Fig. 2B, we plot the total rates of the transitions considered in Fig. 2A [i.e., radiative + nonradiative (solid lines) in addition to the radiative decay rates (dashed lines)]. For low confinement, the nonradiative decay is completely dominant. This reflects the well-known fact that nonradiative energy transfer strongly depends on the ratio $1/(\eta_0 k z_0)$ (29). A similar result of quenching was pointed out in (43). What is more valuable for optical applications is the situation at high confinement. The threshold value of confinement in order to be considered “high confinement” depends on the multipolar order in question. For dipole transitions, high confinement can mean $\eta_0 > 20$. For E5 transitions, it can mean $\eta_0 > 150$.

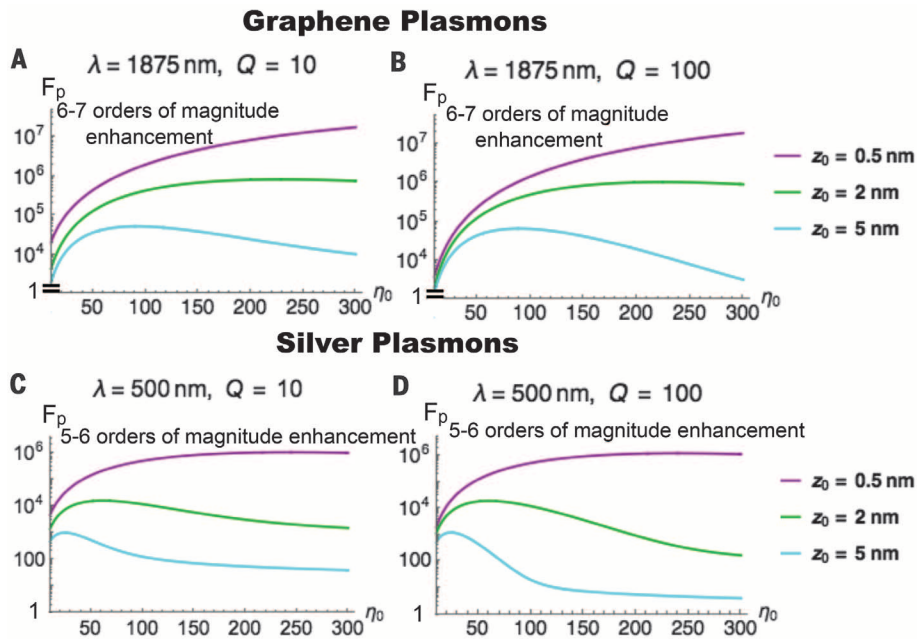


Fig. 3. Enabling singlet-to-triplet transitions. (A to D) Purcell factors for a dipolar singlet-triplet transition as a function of confinement factor η_0 for plasmons in graphene [(A) and (B)] and plasmons in 2D silver [(C) and (D)] for different atom-plane separations z_0 and quality factors Q . These results also apply to other kinds of intercombination transitions, such as those in which the spin of an atomic emitter is flipped because of radiation.

In the high-confinement regime, the radiation into plasmons is dominant and can be harvested as far-field light through suitable outcoupling techniques such as gratings and nanoantennas (39, 44–47).

Spin-flip transitions and the singlet-to-triplet transition

We next analyze those transitions for which the initial state does not directly connect to the final state by the emission of light, but rather couples to a virtual state whose symmetry is compatible with that of the final state. Take as an example a radiative transition between a spin-singlet state S and a spin-triplet state T . The dominant process for systems with large spin-orbit coupling is a second-order process in which an initial triplet state connects to a virtual singlet state S_n through the spin-orbit coupling, and then the virtual state connects to the final singlet state and emits light. The decay rate is then given by the second-order perturbation theory expression

$$\Gamma(T \rightarrow S) = \frac{2\pi}{\hbar^2} \sum_{\mathbf{q}} \left| \sum_n \frac{\langle S, \mathbf{q} | H_{em} | S_n, 0 \rangle \langle S_n, 0 | H_{SO} | T, 0 \rangle}{E_T - E_{S_n}} \right|^2 \times \delta(\omega_{\mathbf{q}} - \omega_0) \quad (5)$$

where ω_0 is the transition frequency and \mathbf{q} is the wave vector of an emitted plasmon.

Use of the Fermi Golden Rule to calculate the decay rate generally involves summation over all possible intermediate states. However, in many cases, there is an intermediate singlet state that

is nearly degenerate with the triplet state, which then gives the dominant contribution to the transition, allowing us to ignore the existence of other singlet states. The advantage of this approximation is that the spin-orbit and electromagnetic enhancements decouple. Our approach allows the calculation of the enhancement factor without knowing anything about the spin-orbit coupling, or even about the structure of the atom or molecule, and thus our results can be applied to many atomic and molecular systems. The Purcell factor, defined as the emission rate into plasmons divided by the emission rate into free-space photons, in the absence of plasmon losses, is proportional to

$$F_p(T \rightarrow S) \sim \eta_0^3 \exp(-2\eta_0 k z_0) \quad (6)$$

where η_0 is the confinement factor at the transition frequency ω_0 , and z_0 is the separation between the atomic nucleus and the surface. For the same reason as discussed previously, the mechanism of this enhancement is purely LDOS-based. This simple formula is only weakly modified by plasmonic losses (for reasons discussed above), which were taken into account in our numerical calculations (29). These high enhancement factors are in agreement with the η_0^3 decay law of pure electric dipole transitions (26, 27).

In Fig. 3, we illustrate the Purcell factors achievable for an emitter on top of graphene and monolayer silver as a function of plasmon confinement. We consider these transitions in a helium-like atom, where the singlet and triplet states (split by electron repulsion) are under-

stood as coming from pairs of one-electron states (29). We show the Purcell factors at distances of 0.5, 2, and 5 nm away for two different plasmon quality factors ($Q = 10$ and $Q = 100$). Figure 3 demonstrates how 2D plasmons can enhance singlet-to-triplet transition by up to seven orders of magnitude for realistic and experimentally readily available parameters. This enhancement is separate from the fact that additional enhancements can come from increasing spin-orbit coupling (5). This allows one to combine approaches involving high spin-orbit coupling and approaches involving plasmonics, thereby allowing attainment of the highest possible enhancements. Perhaps of more interest, it allows one to reconsider the use of emitters with weak spin-orbit coupling. For example, by enhancing the triplet decay by four to six orders of magnitude, one can take a triplet state of a hydrocarbon with a typical phosphorescence time of 0.1 to 0.001 s and make it competitive with, or even faster than, phosphorescence of organometallic triplet states with high spin-orbit coupling.

Another method of enhancing spin-flip and singlet-triplet transitions involves a direct emission into a plasmon through the $\mathbf{S} \cdot \mathbf{B}$ term of the interaction Hamiltonian. Such a direct spin-flip (or singlet-triplet) transition involves an Mn transition, for which the decay rate into plasmons is slower than its electric counterpart by the ratio $\hbar\omega_0/m_e c^2 \approx 10^{-5}$ to 10^{-6} and is thus much slower than the intercombination mechanism for spin-orbit couplings of interest. We demonstrate this claim by deriving rates for Mn transitions (29).

Two-plasmon spontaneous emission

The emission of two excitations of a field (photons or plasmons) is a second-order effect in perturbation theory. If the dimensionless coupling constant g of atomic QED is small, then the two-quanta emission will be very slow relative to the emission of a single field excitation. A good estimate for the coupling constant is given by $g^2 = \Gamma/\omega_0$. When the value of g^2 approaches 1, we expect the Fermi Golden Rule (and more generally, perturbation theory) to fail, because the width of the resulting atomic resonance is comparable to the frequency scale of variation of the continuum matrix elements (48). Taking this as our dimensionless coupling constant, we see that it scales as

$$g_n \sim \sqrt{\alpha(k a_0)^{2n} \eta_0^{3+2(n-1)} \exp(-2\eta_0 k z_0)} \quad (7)$$

in atomic and molecular systems, where a_0 is the characteristic emitter size (for example, the Bohr radius).

For dipole transitions, this coupling constant suggests that the emission rate of two plasmons scales as $g^4 \sim \eta_0^6$. Our rigorous derivation shows that this is indeed the case (29) for both Drude-like and linear plasmon dispersions. Similar conclusions hold for other dispersion relations. We arrive at the following analytical expression for the enhancement of the differential decay rate

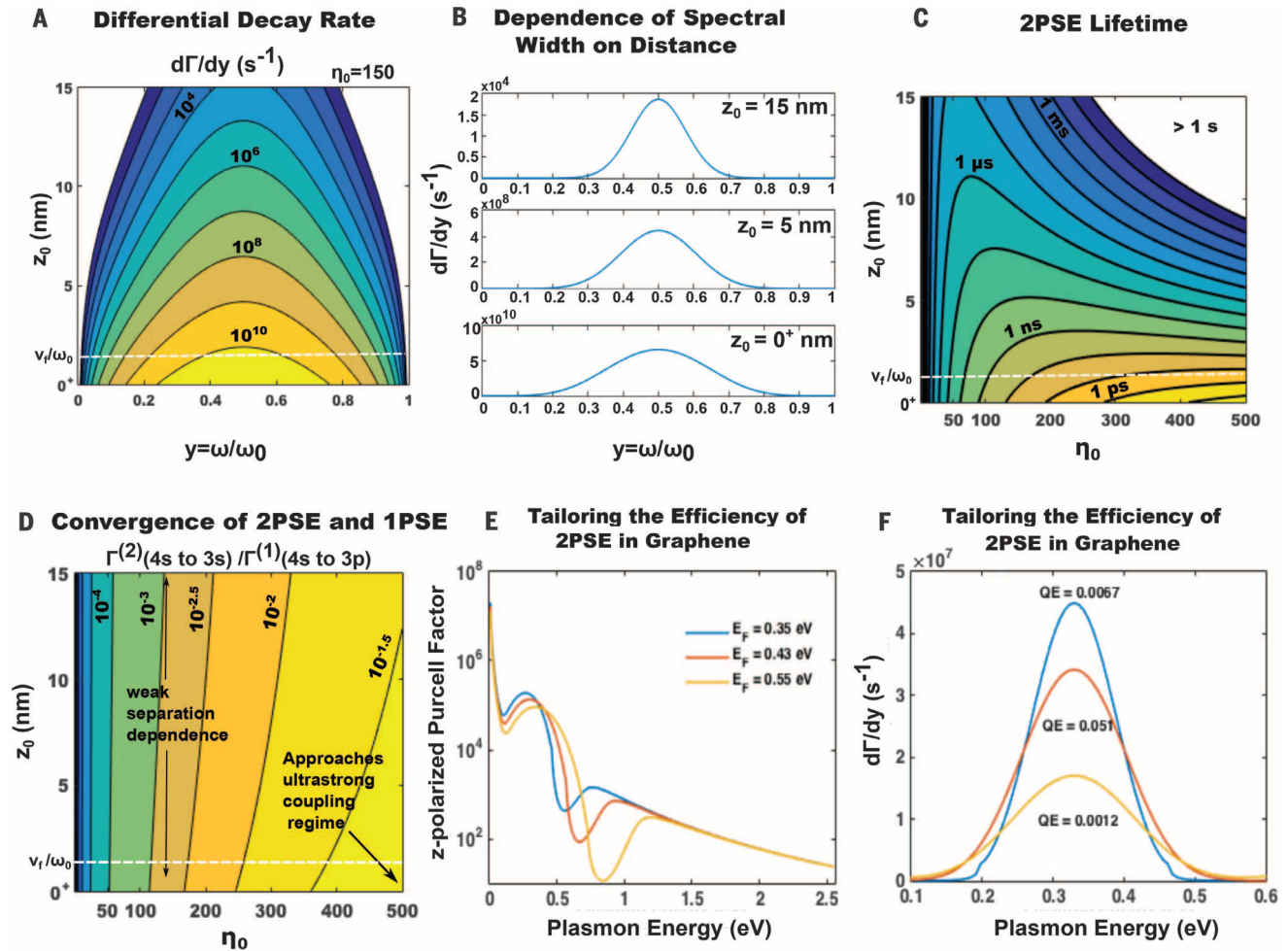


Fig. 4. Enabling two-plasmon radiative energy transfer. (A) Emission spectrum of two-plasmon spontaneous emission (2PSE) as a function of frequency and atom-surface separation for the hydrogen 4s → 3s transition above graphene. η_0 is chosen to be 150. (B) Line cuts of (A) for atom-surface separations of 0, 5, and 15 nm. (C) Total decay rate (in s^{-1}) for this transition as a function of confinement and atom-surface separation. (D) Comparison of two-plasmon emission rate to the emission rate for a single plasmon 4s → 3p

transition as a function of confinement and separation. (E) Purcell spectra for a z-polarized dipole 10 nm from graphene as a function of transition energy for different values of the Fermi energy of graphene. (F) Two-plasmon spontaneous emission spectra as a function of the energy of one of the emitted plasmons for the same values of Fermi energy as in (E). The plots show the transition lifetime and the quantum efficiency of the transition, assuming that the competing transitions (4s → 3p and 4s → 2p) are dipolar.

(in the lossless limit) for any two-plasmon $S \rightarrow S$ transition in a hydrogenic atom:

$$\begin{aligned} \frac{d\Gamma/dy|_{2\text{pl}}}{d\Gamma/dy|_{2\text{ph}}} &= \frac{d\Gamma/d\omega|_{2\text{pl}}}{d\Gamma/d\omega|_{2\text{ph}}} = \\ &= 72\pi^2 [\eta_0^3 \exp(-2\eta_0 k z_0)]^2 \\ &\times (y - y^2)^3 \exp[8\eta_0 k z_0 y(1 - y)] \\ &= \frac{1}{2} F_p(y) F_p(1 - y) \end{aligned} \quad (8)$$

where $y = \omega/\omega_0$, η_0 is the confinement factor at the spectral peak of the emission, and F_p is the Purcell factor for one-plasmon spontaneous emission for a dipole polarized perpendicular to the surface of the 2D conductor. This peak occurs for $\omega = \frac{1}{2}\omega_0$ or, equivalently, $y = \frac{1}{2}$. $d\Gamma/d\omega(\omega')$ corresponds to the rate of emission of two plas-

mons per unit frequency, in which one plasmon is at frequency ω' and the other is at frequency $\omega_0 - \omega'$. A quick estimate using Eq. 8 reveals that at confinement factors of 200, the left side of Eq. 8, defined as the spectral enhancement, tends to 10^{15} as $z_0 \rightarrow 0$. The $\frac{1}{2}F_p(y)F_p(1 - y)$ term of Eq. 8 reveals the mechanism of two-plasmon spontaneous emission enhancement: LDOS enhancement over a sufficiently broad frequency spectrum such that enhancement at complementary frequencies, ω and $\omega_0 - \omega$, is very high. For Fig. 4, A to D, we consider two-plasmon spontaneous emission without considering losses. We discuss the effect of plasmon losses below.

In Fig. 4A, we plot the distribution of emitted plasmons as a function of normalized frequency, y . The spectral distribution narrows for increasing atom-surface separation z_0 (Fig. 4B). This arises from the y dependence of the exponential in Eq. 8. Therefore, through a precise control of

the position of an emitter above a surface supporting plasmons, it is possible to tune not only the rate of emission, but also the spectrum of emission.

In Fig. 4C, we plot an estimate of the total decay rate for the transition 4s → 3s, which is computed by summing over 10 virtual discrete states (29). The rate converges sufficiently for 10 virtual states. Even for modest confinements of around 100, and at separations of 5 nm, the two-plasmon spontaneous emission rate approaches 0.1 ns^{-1} , in stark contrast to the typical rate of roughly 1 min^{-1} in free space. For confinements beyond 200, it is possible to obtain plasmon emission rates exceeding 0.1 ps^{-1} . We compare the rate of this transition with that of the 4s → 3p single-plasmon dipole transition in Fig. 4D; in the region of extreme confinement (200 to 500), the two-plasmon emission is only one to two orders of magnitude slower. At these extreme confinements—such that the two-plasmon emission is slower than the

one-plasmon emission by two orders of magnitude—the dimensionless coupling constant g is on the order of 0.1, signaling the onset of the ultrastrong coupling regime.

We find that for plasmons described by the Drude model, the ratio of the rates has a very weak distance dependence. This arises from the fact that at greater atom-surface separations, the spectrum of emitted plasmons gets narrower. Therefore, most of the emitted plasmons have frequencies near $\gamma = 1/2$. When this happens, the distance dependence of the two-plasmon decay rate approaches $\exp(-2\eta_0 kz_0)$, which is the same distance dependence as that of the one-plasmon decay rate. This is a feature of the $\omega \sim \sqrt{q}$ dispersion of plasmons, which is well described by the Drude model. For plasmons with linear dispersion (such as acoustic plasmons), the distance dependence of the two-plasmon differential emission rate is simply $\exp(-4\eta_0 kz_0)$ (i.e., no γ dependence, in contrast to that of Eq. 8). The results summarized in Fig. 4, A to D, establish that two-plasmon spontaneous emission is very fast in the vicinity of 2D plasmon-supporting materials. Indeed, it should already be experimentally achievable to observe lifetimes for two-plasmon processes on the order of 1 ns, which is of similar order of magnitude to that of fast dipole transitions in free space. We note that the effect of losses is considered in our study (29). In brief, for this particular transition, second-order quenching effects are only of extreme relevance at very short atom-surface separations of below 1 nm (see Fig. 4, E and F, and fig. S4 to see how the results in Fig. 4, A to D, are modified by losses). However, our consideration of losses opens up the possibility of observing and potentially using a new decay mechanism for emitters near a surface: nonradiative decay through two (entangled) lossy excitations (i.e., double quenching).

Next, we show that it is even possible to exceed the efficiencies for two-plasmon emission suggested by Fig. 4D, allowing for the possibility of efficient sources of entangled plasmons. It is known both theoretically (27) and experimentally (20) that graphene features a spectral region (roughly) between E_F and $2E_F$ in which the Purcell factor drops by several orders of magnitude. We call this region the “dip region.” Consider a hydrogenic electron in the 4s state. The 4s can decay into the 2p and 3p states by first-order emission. It can also potentially decay into 3s via two-plasmon spontaneous emission. All other processes are negligible. Suppose that the energy difference between 4s and 3s (0.66 eV) lies within the spectral dip region. Further suppose that highly confined plasmons exist at 0.33 eV. Then, the relative enhancement between second order and first order emission processes will be much higher than suggested by Fig. 4D, which assumed no such dip. In Fig. 4E, we show the Purcell factor for first-order (dipolar) emission for a z -polarized dipole at atom-surface separation of 10 nm for graphene Fermi energies of 0.35, 0.43, and 0.55 eV. Our calculations take the spatial nonlocality of graphene’s permittivity into account via the RPA,

as is done in (15, 27). In Fig. 4F, we show the spectrum of plasmon emission (which is integrated to get the overall transition rates) and quantum efficiencies for two-plasmon spontaneous emission at these different atom-surface separations (49). The quantum efficiency here is well approximated by

$$QE = \frac{\Gamma(4s \rightarrow 3s)}{\Gamma(4s \rightarrow 3s) + \Gamma(4s \rightarrow 3p) + \Gamma(4s \rightarrow 2p)} \quad (9)$$

We find that the quantum efficiency of two-plasmon emission is an extremely strong function of Fermi energy, jumping by an order of magnitude as E_F is varied from 0.35 eV to 0.43 eV and as E_F is varied from 0.43 eV to 0.55 eV. At $E_F = 0.43$ eV, the quantum efficiency of two-plasmon emission is 5%, which is not only quite high for a second-order process, but is also far larger than what is suggested by Fig. 4D, and it is enabled as a result of the spectral dip in graphene. Therefore, using low-loss plasmons such as those observed recently in graphene (27) and the results presented here, one may be able to generate and couple out entangled plasmons at a fast rate and at a relatively high efficiency. These findings suggest very clearly that it should be possible to use systems with high Purcell factors over a narrow spectral region to enhance the relative efficiency of multipolar and spin-flip transitions as well (although not in the highly degenerate hydrogen atom). Other systems with high Purcell factors over a narrow spectral region through which our findings may be realized include nanometer-scale plasmonic resonators with high quality factors and few-nanometer-thick metallic thin films.

Summary and outlook

We have shown that 2D plasmonics, with its unprecedented level of confinement, presents a unique opportunity to access radiative transitions in atomic-scale emitters that were considered inaccessible. Multiplasmon processes, spin-flip radiation, and very high-order multipolar processes have been shown to be competitive with

the fastest atomic transitions in free space, rendering them all accessible. These findings (Table 1) pave the way to observing and taking advantage of new light-matter interactions. In particular, our findings may force the reconsideration of many atomic, molecular, and solid-state emitters whose transitions are normally too weak and inefficient to be used, thus bringing the full variety of the periodic table to optical applications. The physics responsible for the effects reported here may also be present in optical antennas whose dimensions are on the order of 1 nm (50). However, even if they are, an advantage of planar 2D plasmonics for accessing forbidden transitions is that the effect does not depend on the position of the emitter in the plane parallel to the 2D conductor. In cavity-based emission enhancement platforms, especially those in which fields are confined in a few-nanometer gap, the (atomic-scale) emitter must be positioned very precisely in order to observe the enhancement.

In many cases, we found that quenching was a weak correction to the decay of the emitters and that the primary decay was into propagating (albeit lossy) plasmons, which could be coupled out into far-field photons. Thus, the presence of forbidden transitions can be translated into far-field photons at frequencies not in the conventional emission spectrum of the emitter. Thus, one could experimentally observe forbidden transitions (and infer their rates) indirectly through these unconventional far-field photons. Note that even if the plasmons could not be outcoupled—for example, because of debilitatingly high losses—there will often be clear experimental signatures of these transitions. In particular, because some of the transitions will primarily occur via emission of a far-field photon, the presence of forbidden decay pathways will modify the far-field spectrum of an emitter, and a quantitative knowledge of the modified far-field emission spectrum of the emitter will allow one to infer the presence of forbidden transitions and the type of forbidden transition taking place. In fig. S5, we show

Table 1. A summary of derived scalings of rates and rate enhancements for emitters on top of lossless 2D plasmons at zero displacement from the plasmon-supporting surface. The rates for an emitter at finite distance from the plasmon are suppressed by factors of $\exp(-2\eta_0 kz_0)$, which is of order unity for an emitter within a reduced plasmon wavelength of the surface. Note that these scalings are still a good approximation even in the presence of high losses, provided that the confinement is large (Fig. 2). 2PSE, two-plasmon spontaneous emission.

Transition*	Free space Γ	2D plasmon Γ	η Enhancement
E1	$\alpha(\hbar\omega/m_e c^2)$	$\alpha(\hbar\omega/m_e c^2)\eta^3$	3
E_n	$\alpha(\hbar\omega/m_e c^2)(ka_0)^{2(n-1)}$	$\alpha(\hbar\omega/m_e c^2)(ka_0)^{2(n-1)}\eta^{3+2(n-1)}$	$3 + 2(n - 1)$
Spin-flip $E_k \uparrow$	$\alpha(\hbar\omega/m_e c^2)(ka_0)^{2(n-1)}$	$\alpha(\hbar\omega/m_e c^2)(ka_0)^{2(n-1)}\eta^{3+2(n-1)}$	$3 + 2(n - 1)$
2PSE (dipole)	$\alpha^2(ka_0)^4$	$\alpha^2(ka_0)^4\eta^6$	6
$M1 \uparrow$	$\alpha(\hbar\omega/m_e c^2)^2$	$\alpha(\hbar\omega/m_e c^2)^2\eta$	1
$Mn \uparrow$	$\alpha(\hbar\omega/m_e c^2)^2(ka_0)^{2(n-1)}$	$\alpha(\hbar\omega/m_e c^2)^2(ka_0)^{2(n-1)}\eta^{1+2(n-1)}$	$1 + 2(n - 1)$

*Losses can change these significantly at low confinement and/or short separation.

†Not including the spin-orbit matrix element, which approximately does not contribute to the Purcell enhancement.

‡M1 and Mn are discussed in (29).

an energy-level diagram in an emitter conducive to observing forbidden transitions, even without outcoupling.

With regard to applications of this work to fundamental light-matter interactions, we believe that a number of fruitful extensions are within reach. Beyond the processes that we considered in this work, one can consider combinations of these processes, such as (i) multiplasmon transitions mediated by higher-order multipole virtual transitions, such as a two-plasmon emission with a total angular momentum change of 4 for the electron by way of intermediate quadrupole virtual transitions; (ii) third- and higher-order plasmon emission and absorption processes; or (iii) a second-order absorption process in which a plasmon and a far-field photon are absorbed, leading to large changes in energy and angular momentum of the electron due to the photon and plasmon, respectively.

All of these transitions should be enhanced using 2D plasmonics, but beyond the reach of conventional plasmonics and photonics without extremely high intensities of light. We stress that the results we have presented are not optimized. We performed our work with hydrogen purely as a proof-of-concept. For example, by finding an atom with a high octupole moment, it should be possible to make the octupole transition dominant over the dipole and other multipolar transitions, thereby paving the way for emitters with characteristic multipolarity different from dipolar. It should similarly be possible to optimize the rate of multiplasmon spontaneous emission relative to other transitions, leading to emitters highly capable of emitting entangled light.

Potential applications of this work include spectroscopy for inferring electronic transitions that cannot be determined with photons, sensors based on forbidden transitions, organic light sources arising from fast singlet-triplet transitions, fast entangled light generation, and fast generation of broadband light with tunable width in the near- and mid-infrared. Many of these applications could also be realized with the highly dissipative visible-frequency excitations in 2D conductors.

REFERENCES AND NOTES

1. P. A. Dirac, *Proc. R. Soc. London Ser. A* **114**, 243–265 (1927).
2. M. Pelton, *Nat. Photonics* **9**, 427–435 (2015).
3. M. Tame et al., *Nat. Phys.* **9**, 329–340 (2013).
4. R. Friend et al., *Nature* **397**, 121–128 (1999).
5. A. Köhler, H. Bässler, *Mater. Sci. Eng. Rep.* **66**, 71–109 (2009).
6. M. Göppert, *Naturwissenschaften* **17**, 932 (1929).
7. C. L. Cesar et al., *Phys. Rev. Lett.* **77**, 255–258 (1996).
8. A. Hayat, P. Ginzburg, M. Orenstein, *Nat. Photonics* **2**, 238–241 (2008).
9. A. Nevet et al., *Nano Lett.* **10**, 1848–1852 (2010).
10. A. Hayat, A. Nevet, P. Ginzburg, M. Orenstein, *Semicond. Sci. Technol.* **26**, 083001 (2011).
11. T. Nagao, T. Hildebrandt, M. Henzler, S. Hasegawa, *Phys. Rev. Lett.* **86**, 5747–5750 (2001).
12. B. Diaconescu et al., *Nature* **448**, 57–59 (2007).
13. Y. Liu, R. Willis, K. Emtsev, T. Seyller, *Phys. Rev. B* **78**, 201403 (2008).
14. E. Rugeramigabo, T. Nagao, H. Pfür, *Phys. Rev. B* **78**, 155402 (2008).
15. M. Jablan, H. Buljan, M. Soljačić, *Phys. Rev. B* **80**, 245435 (2009).
16. S. J. Park, R. E. Palmer, *Phys. Rev. Lett.* **105**, 016801 (2010).
17. A. Grigorenko, M. Polini, K. Novoselov, *Nat. Photonics* **6**, 749–758 (2012).
18. Z. Fei et al., *Nature* **487**, 82–85 (2012).
19. M. Jablan, M. Soljačić, H. Buljan, *Proc. IEEE* **101**, 1689–1704 (2013).

20. K. Tielrooij et al., *Nat. Phys.* **11**, 281–287 (2015).
21. A. Woessner et al., *Nat. Mater.* **14**, 421–425 (2015).
22. Q. Zhang et al., *Sci. Rep.* **4**, 6559 (2014).
23. Z. Fei et al., *Nano Lett.* **11**, 4701–4705 (2011).
24. H. Yan et al., *Nat. Photonics* **7**, 394–399 (2013).
25. E. Altewischer, M. P. van Exter, J. P. Woerdman, *Nature* **418**, 304–306 (2002).
26. A. Archambault, F. Marquier, J.-J. Greffet, C. Arnold, *Phys. Rev. B* **82**, 035411 (2010).
27. F. H. Koppens, D. E. Chang, F. J. García de Abajo, *Nano Lett.* **11**, 3370–3377 (2011).
28. L. Gaudreau et al., *Nano Lett.* **13**, 2030–2035 (2013).
29. See supplementary materials on Science Online.
30. We expect nonlocal effects to kick in at atom-surface separations $z_0 \leq v_F/\omega_0$, where v_F is the Fermi velocity and ω_0 is the transition frequency.
31. A. Kramida et al., Atomic Spectra Database (National Institute of Standards and Technology, Gaithersburg, MD, 2012).
32. J. R. Zurita-Sánchez, L. Novotny, *J. Opt. Soc. Am. B* **19**, 1355 (2002).
33. J. R. Zurita-Sánchez, L. Novotny, *J. Opt. Soc. Am. B* **19**, 2722 (2002).
34. R. Filter, S. Mühlig, T. Eichelkraut, C. Rockstuhl, F. Lederer, *Phys. Rev. B* **86**, 035404 (2012).
35. M. Takase et al., *Nat. Photonics* **7**, 550–554 (2013).
36. V. Yannopoulos, E. Paspalakis, *J. Mod. Opt.* **62**, 1435–1441 (2015).
37. M. L. Andersen, S. Stobbe, A. S. Sørensen, P. Lodahl, *Nat. Phys.* **7**, 215–218 (2011).
38. I. D. Rukhlenko et al., *Opt. Express* **17**, 17570–17581 (2009).
39. P. K. Jain, D. Ghosh, R. Baer, E. Rabani, A. P. Alivisatos, *Proc. Natl. Acad. Sci. U.S.A.* **109**, 8016–8019 (2012).
40. G. M. Akselrod et al., *Nat. Photonics* **8**, 835–840 (2014).
41. Technically, $\nabla \cdot \mathbf{E} \neq 0$ only at the surface, but the contribution is small because the atomic wave functions are exponentially suppressed at the surface, so for parameters of interest, the direct $s \rightarrow s$ transition is much weaker than the two-plasmon process.
42. A. F. Page, F. Ballout, O. Hess, J. M. Hamm, *Phys. Rev. B* **91**, 075404 (2015).
43. A. Alabastri, X. Yang, A. Manjavacas, H. O. Everitt, P. Nordlander, *ACS Nano* **10**, 4835–4846 (2016).
44. G. Liu et al., *ACS Nano* **6**, 6786–6792 (2012).
45. A. N. Abbas et al., *ACS Nano* **8**, 1538–1546 (2014).
46. T. B. Hoang et al., *Nat. Commun.* **6**, 7788 (2015).
47. For applications in which fast nonradiative decay is desired, we note that for considerably low wavelengths $1/kz_0 = 1$, the

nonradiative decay is much faster than one would naively expect. This is because the nonradiative decay still couples to the multipole moment relevant to the atomic transition. Therefore, the strong enhancement of rates coming from matching the atomic size to the wavelength of light compensates for the suppression of rates coming from a higher kz_0 . In fact, the total rate—even when nonradiative energy transfer is dominant—increases as the wavelength shrinks. From this, we conclude that for both radiative and nonradiative decay, the high confinement of 2D plasmons helps to overcome the small size of the atom.

48. C. Cohen-Tannoudji, J. Dupont-Roc, G. Grynberg, P. Thickstun, *Atom-Photon Interactions: Basic Processes and Applications* (Wiley, 1992).
49. We note that in principle the spectra increase for low frequencies because of quenching, but in the cases presented, it only provides a weak logarithmic correction to the decay rates (one to two orders of magnitude below the computed decay rates in Fig. 4F). This logarithmic correction is regulated by the energy difference between 4s and 4p levels (due to the Lamb shift). In other atoms, it is regulated by a much larger frequency (due to the lack of degeneracy between s and p orbitals), making the correction even weaker than in hydrogen (29).
50. A. Alù, N. Engheta, *Nat. Photonics* **2**, 307–310 (2008).

ACKNOWLEDGMENTS

Supported by S3TEC, an Energy Frontier Research Center funded by U.S. Department of Energy grant DE-SC0001299 (B.Z. and M.S.); Marie Curie grant 328853-MC-BSICS (I.K.); and the Army Research Office through the Institute for Soldier Nanotechnologies under contract W911NF-13-D-0001. We thank P. Rebusco for critical reading and editing of the manuscript, and H. Buljan, K. Nelson, O. Shapira, and J. Lopez for useful discussions. The authors and MIT have filed U.S. patent applications 62/342,287 and 62/266,762 that relate to the mechanisms described in this manuscript.

SUPPLEMENTARY MATERIALS

www.sciencemag.org/content/353/6296/263/suppl/DC1
Figs. S1 to S5
References (51–55)

6 March 2016; accepted 17 June 2016
10.1126/science.aaf6308

OZONE HOLE

Emergence of healing in the Antarctic ozone layer

Susan Solomon,^{1*} Diane J. Ivy,¹ Doug Kinnison,² Michael J. Mills,² Ryan R. Neely III,^{3,4} Anja Schmidt³

Industrial chlorofluorocarbons that cause ozone depletion have been phased out under the Montreal Protocol. A chemically driven increase in polar ozone (or “healing”) is expected in response to this historic agreement. Observations and model calculations together indicate that healing of the Antarctic ozone layer has now begun to occur during the month of September. Fingerprints of September healing since 2000 include (i) increases in ozone column amounts, (ii) changes in the vertical profile of ozone concentration, and (iii) decreases in the areal extent of the ozone hole. Along with chemistry, dynamical and temperature changes have contributed to the healing but could represent feedbacks to chemistry. Volcanic eruptions have episodically interfered with healing, particularly during 2015, when a record October ozone hole occurred after the Calbuco eruption.

Antarctic ozone depletion has been a focus of attention by scientists, policy-makers, and the public for three decades (1). The Antarctic ozone hole opens up in austral spring of each year and is measured both by its depth

(typically a loss of about half of the total integrated column amount) and its extent (often more than 20 million km² by October). Ozone losses have also been documented in the Arctic and at mid-latitudes in both hemispheres (2). Concern



Shrinking light to allow forbidden transitions on the atomic scale

Nicholas Rivera, Ido Kaminer, Bo Zhen, John D. Joannopoulos and Marin Soljacic (July 14, 2016)
Science **353** (6296), 263-269. [doi: 10.1126/science.aaf6308]

Editor's Summary

Making the forbidden allowed

Spontaneous emission, in which an excited electron lowers its energy by emitting a photon, is a fundamental process in light-matter interactions. In principle, the electron can relax from the excited state to any unoccupied lower energy level. In practice, however, most of these transitions are too slow and so are effectively forbidden. Rivera *et al.* show theoretically that the plasmonic excitations associated with two-dimensional materials can be used to enhance and control the light-matter interaction. Transitions that were once considered forbidden can thus be accessed, opening up the entire spectrum of an optical emitter.

Science, this issue p. 263

This copy is for your personal, non-commercial use only.

Article Tools Visit the online version of this article to access the personalization and article tools:
<http://science.sciencemag.org/content/353/6296/263>

Permissions Obtain information about reproducing this article:
<http://www.sciencemag.org/about/permissions.dtl>

Science (print ISSN 0036-8075; online ISSN 1095-9203) is published weekly, except the last week in December, by the American Association for the Advancement of Science, 1200 New York Avenue NW, Washington, DC 20005. Copyright 2016 by the American Association for the Advancement of Science; all rights reserved. The title *Science* is a registered trademark of AAAS.